International Journal of Mechanical Sciences 268 (2024) 109021

Contents lists available at ScienceDirect

International Journal of Mechanical Sciences

journal homepage: www.elsevier.com/locate/ijmecsci

Surface roughening and hemi-wicking: Synergistic impact on flow boiling

Geehong Choi [a,1,2], Beom Seok Kim [b,1], Maroosol Yun [a], Namkyu Lee [a], Sangwoo Shin [c], Hyung Hee Cho [a,*]

[a] Department of Mechanical Engineering, Yonsei University, 03722 Seoul, Korea
[b] Department of Mechanical and Automotive Engineering, Seoul National University of Science and Technology, 01811 Seoul, Korea
[c] Department of Mechanical and Aerospace Engineering, University at Buffalo, The State University of New York, Buffalo, NY 14260, USA

ARTICLE INFO

Keywords:
Flow boiling heat transfer
Nanowires
Hemi-wicking
Surface roughening
Critical heat flux
Bubble pinning

ABSTRACT

This study advances thermal management in flow boiling by investigating the synergy between nanoscale surface structures, hemi-wicking, and bubble dynamics during phase changes, with a particular focus on innovative surface morphology. Nanowires, known for enhancing heat transfer through surface roughening and interfacial wicking, play a crucial role. We highlight the importance of morphological roughening and its synergy with hemi-wicking in enhancing critical heat flux (CHF) in flow boiling. We demonstrate that surfaces functionalized with vertical silicon nanowires show a significant increase in CHF compared to smooth surfaces. This enhancement is attributed to improved liquid supply and prevention of bubble pinning, thus maximizing heat dissipation. However, the absence of hemi-wicking on nano-inspired surfaces unexpectedly leads to a substantial CHF reduction compared to smooth counterparts. By visualizing bubble dynamics under forced convection, we reveal the critical role of hemi-wicking in sustaining continuous liquid supply and postponing the onset of film boiling by ensuring an anti-pinning effect of bubbles. These findings offer valuable insights into interface functionalization and surface morphology design for efficient heat dissipation, emphasizing the often-overlooked role of hemi-wicking in preventing bubble pinning. This knowledge is pivotal for developing compact and high-efficiency cooling technologies.

1. Introduction

Boiling is a pivotal heat transfer mode extensively utilized in diverse engineering systems, including electronic devices, power plants, photovoltaics, and aerospace technology, due to its significant energy transfer capability. This capability is attributed to the high convective heat transfer coefficient during two-phase convection [1–8]. Despite its advantages, the application of boiling is constrained by the critical heat flux (CHF), a parameter limiting the maximum allowable heat dissipation capacity [8–11]. The CHF mechanism is influenced by surface characteristics, such as surface roughening and liquid accessibility (Fig. 1). Previous studies have demonstrated that these factors can delay film boiling, providing hydraulic and thermal stability between vaporization through nucleation and the counteracting liquid supply [12–15].

Recent advances in *functionalized interfacial structures*, including micropatterns, nanostructures, hierarchical structures, and graphene-coated structures, have significantly enhanced boiling heat transfer performances [13,16-25] with some efforts increasing CHF by over 100% [26–29]. However, these advancements have yet to fully address the complex interplay between surface characteristics and boiling heat transfer, leaving a significant gap in understanding, particularly in the context of nanostructured surfaces. The 'classical' approaches, focusing on primary variables such as roughness and wettability [15,30-33], are limited in their capacity to fully elucidate the contribution of innovative functional structures to CHF improvement [10,13,34]. Consequently, a comprehensive exploration of the synergistic effects between surface roughness and wettability is essential to offer novel insights into CHF improvement.

The contact angle (CA) of a working fluid determines the liquid accessibility, and thus the hydraulic continuity of a boiling interface [14, 34-36]. The CA is sensitive to surface roughness where the apparent CA θ is characterized by the roughness factor r (the ratio of the actual surface area to the projected one) in the form of $\cos\theta = r\cdot\cos\theta^*$ where θ^* is the CA on an ideal smooth surface [37–40]. Wenzel's model elucidates that an increase in surface roughness enhances hydrophilicity [41].

* Corresponding author.
E-mail address: hhcho@yonsei.ac.kr (H.H. Cho).
[1] These authors contributed equally to this work as the first authors.
[2] Current address: Hyundai Steel Co. Ltd., Chungcheongnam-do, Korea

https://doi.org/10.1016/j.ijmecsci.2024.109021
Received 17 October 2023; Received in revised form 5 January 2024; Accepted 5 January 2024
Available online 11 January 2024

Nomenclature

Symbols

A_{heater}	heating area (m^2)
H	height of the interfacial structure (m)
h	latent heat of liquid-vapor phase (J/g)
I	current (A)
k_{Si}	thermal conductivity of the Si substrate (W/m·K)
L	total channel length
L_d	fully developed length along the channel
Q	applied power (W)
Q_{loss}	loss of the applied power (W)
q''	heat flux, CHF (W/cm^2)
q''_{CHF}	critical heat flux, CHF (W/cm^2)
$q''_{CHF,0}$	critical heat flux on a planar surface predicted by Kandlikar's model (W/cm^2)
R_a	arithmetic average roughness (nm)
R_q	root mean square roughness (nm)
r	surface roughness factor
T_{RTD}	temperature measure from the RTD (K)
T_{wall}	wall temperature on the boiling surface (K)
t_{Si}	thickness of the Si substrate
V	voltage drop (V)
W	wicking rate ($mm/s^{0.5}$)

Greek symbols

β	shape factor
θ	apparent contact angle (°)
θ^*	contact angle on an ideal smooth surface (°)
θ_c	critical contact angle (°)
λ_{RT}	Rayleigh-Taylor wavelength (mm)
μ	dynamic viscosity (mPa·s)
φ	solid fraction
ρ_L	liquid density (g/mm^3)
σ	liquid-gas surface tension (mN/m)
σ_{SG}	solid-gas surface tension (mN/m)
σ_{SL}	solid-liquid surface tension (mN/m)

Abbreviations

CA	contact angle (°)
CFD	computational fluid dynamics
CHF	critical heat flux (W/m^2)
CMC	critical micelle concentration
DC	direct current
DI	deionized
ITO	indium–tin–oxide
MEMS	microelectromechanical system
PEEK	polyether ether ketone
RTDs	resistive temperature detectors
Si	silicon
SiNWs	silicon nanowires
Re	Reynolds number

Importantly, the interplay between surface roughness and CA is crucial in improving CHF. Furthermore, recent studies have stressed the importance of "hemi-wicking" for liquid accessibility [4,38,42-46]. Hemi-wicking is the morphologically induced dynamic spreading of a liquid through a roughened interface on a surface by capillary pressure [43,44,47,48]. Stronger interaction between a solid and liquid (low surface energy) than between a solid and vapor (high surface energy) causes the liquid to move forward along the solid-vapor interface. As illustrated in Fig. 1c, hemi-wicking stabilizes the fluid around a bubble during a phase change by supplementing the liquid supply. Hemi-wicking may be a key factor in extending the CHF, which occurs when the mass balance between the vaporized bubbles and the counteracting liquid supply is disrupted [9,10,49]. A recent CHF model suggested incorporating the hemi-wicking effect into the existing hydraulic CHF model:

$$q''_{CHF} = q''_{CHF,0} + \beta h \rho_L (1-\varphi) W^2 \Big/ \lambda_{RT}^2, \quad (1)$$

where β, h, ρ_L, φ, W, λ_{RT}, and $q''_{CHF,0}$ are the shape factor, latent heat, liquid density, solid fraction, wicking rate, Rayleigh–Taylor wavelength, and CHF on a planar surface predicted by Kandlikar's model [10,14], respectively. However, hemi-wicking is not an independent factor; instead, it depends on the morphology and hydrodynamic properties [42,43].

This research introduces a novel approach by deeply exploring the interaction between surface roughness and hemi-wicking using silicon nanowires (SiNWs), presenting an innovative methodology for enhancing CHF. In this study, our primary aim is to dissect the synergistic effects of surface roughness and hemi-wicking in flow boiling. Through the utilization of nanostructured surfaces like SiNWs, we seek to uncover the nuanced roles these factors play in CHF enhancement. This focus on the intricate relationship between surface morphology and liquid dynamics represents a significant advancement in the field, potentially leading to more effective strategies for thermal management in high heat flux applications. Vertically aligned silicon nanowires (SiNWs) were utilized to maximize surface roughness. By reducing the liquid surface tension, we controlled the hemi-wicking to elucidate the distinct role of roughness, effectively decoupling it from hemi-wicking. Our findings highlight the importance of bolstering the liquid supply, especially via hemi-wicking, to prevent bubble pinning. This prevention is crucial as bubble pinning subsequently leads to bubble coalescence and growth, ultimately diminishing the CHF for boiling heat transfer.

2. Materials and methods

This section outlines the methodologies and materials used in our study. It details the fabrication of the sensor with a thin-film heater for local temperature measurement, preparation of SiNWs for the boiling surfaces, and the setup of the flow boiling experiment. Additionally, we describe the procedures for liquid accessibility characterization and data reduction methods employed to evaluate local heat transfer. This comprehensive approach enables a thorough understanding of the experimental setup, ensuring the reliability and validity of our findings.

2.1. Local characterizing sensor with a thin-film heater

To supply heat to and measure the wall temperature on a boiling surface, a thin-film heater and resistive temperature detectors (RTDs) were fabricated on a Si substrate by using a microelectromechanical system (MEMS) process [5,50-52]. The fabricated sensor chip and detailed image for the arrayed five RTDs are presented in Fig. 2a. The heater and RTD sensors were fabricated on a p-type Si substrate (boron-doped; (100) orientation; resistivity: 1–10 Ω·cm; thickness: 500 μm). In addition to the fabrication details, it is important to note that the plain surface of the Si substrate used in our experiments was characterized for its surface roughness. We utilized double-side polished silicon wafers to ensure a smooth surface. Atomic Force Microscopy (AFM) measurements at five random locations on the sample surface revealed an average roughness R_a and R_q of approximately 0.1108 nm and 0.1392 nm, respectively. These results confirm the uniform and minimal surface

roughness of the plain silicon wafers, essential for accurate boiling heat transfer studies.

For the fabrication, first, the Si substrate was cleaned with a piranha solution (3:1 mixture of H_2SO_4 and H_2O_2 by volume) for more than 40 min. It was then cleaned with acetone and methanol for 5 min each in sequence using a sonicator. On the cleaned Si substrate surface, four-wire RTD sensors were patterned by a Pt layer using a lift-off process. The resistance of platinum (Pt) showed a linear response to an increase in temperature. The sensors were calibrated to determine the resistance–temperature relationship. On the RTD layer, an oxide–nitride–-oxide multi-layer was deposited to insulate the RTD sensors from the heater. The heater consists of a 5 × 10 mm^2 indium–tin–oxide (ITO) layer (thickness: 800 nm). Beneath this heater, a series of five RTD sensors are positioned, aligned in a row with a spacing of 1.5 mm apart. Heater electrodes were located at both ends of the heater. The current was supplied to the heater through copper bus bars by a direct current (DC) power supply (200 V-10 A, KSC Korea Switching).

2.2. Preparation of SINW

Fig. 2b displays vertically aligned SiNWs prepared for boiling surfaces. The SiNWs were synthesized using a metal-assisted chemical wet etching method [49,53-56]. The SiNWs were prepared on the rear surface of a silicon chip, equipped with a thin-film heater and resistance-temperature-detector (RTD) sensors for local and transient wall temperature measurement. The silicon substrate underwent a cleaning process to remove organic residues and the native oxide layer. The backside of the sensor was selectively coated with Ag^+ using a mixture of 5 mM $AgNO_3$ and 4.8 M HF solution. This process facilitated the formation of SiNWs on the surface, with their height controlled by the etching time. For this study, SiNWs with an average height of 6.8 μm were obtained after a 30-minute etching process. Details on the fabrication of the RTD sensors with *in situ* SiNWs presented in Fig. 2b are provided our previous report [24,56].

2.3. Flow boiling experiments

Fig. 2c illustrates the closed-loop flow boiling facility, including a test section. The flow boiling test section was made of polyether ether ketone (PEEK) and consisted of inlet and outlet settling chambers and a main channel comprising upper and bottom parts. In each of the inlet and outlet settling chambers, K-type thermocouples (Omega Co.) were installed to measure the temperature of the working fluid. The flow channel had a cross-sectional area of 5 × 5 mm^2, with a total channel length (L) of 375 mm. The fully developed region (L_d) had a length of 200 mm, which was sufficient under turbulent flow conditions [5,52,57]. The fully developed fluid passes over a heating surface with an area of 5 × 10 mm^2 (*i.e.*, the area of the ITO thin film heater on the sensor) to reach a boil. Two types of heating surfaces were used in this study: a smooth (plain) silicon surface and a surface roughened by the *in-situ* formation of vertically aligned monolithic silicon nanowires (SiNWs). Experiments were conducted on both smooth and SiNW-forested surfaces using deionized (DI) water, with a controlled flow condition at Re = 12,000, at saturated conditions (100 °C) and ambient pressure (1 atm). In this study, we selected a Reynolds number of 12,000 to establish a stable turbulent flow, essential for accurately observing nanoscale surface effects such as hemi-wicking. This decision was informed by the need for uniform flow characteristics and minimizing external variables

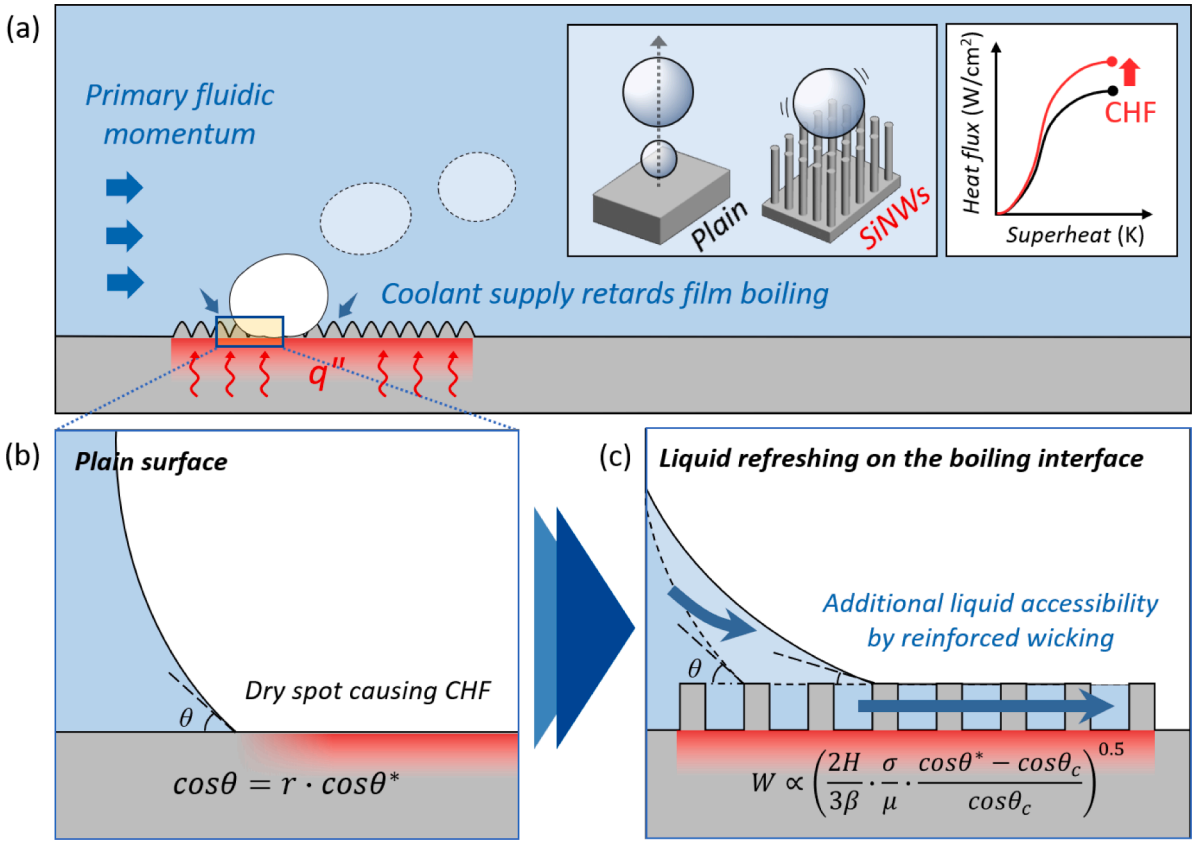

Fig. 1. Illustration of the impact of interfacial characteristics on the critical heat flux (CHF). (a) Bubble behavior on a roughened surface in convective boiling, with insets showing the role of nanowire surfaces and highlighting the interface's role in enhancing CHF, as presented by the boiling curves. (b) Dipiction of liquid accessibility in terms of static contact angle (CA) θ, where r and θ^* are the roughness factor and CA on an ideal smooth surface, respectively. (c) Illustration of enhanced liquid accessibility facilitated by hemi-wicking. The extent of hemi-wicking is quantified by the wicking coefficient W, where H, β, σ, μ and θ_c are height of the interfacial structures, shape factor, surface tension of the fluid, dynamic viscosity of the fluid, and critical CA, respectively.

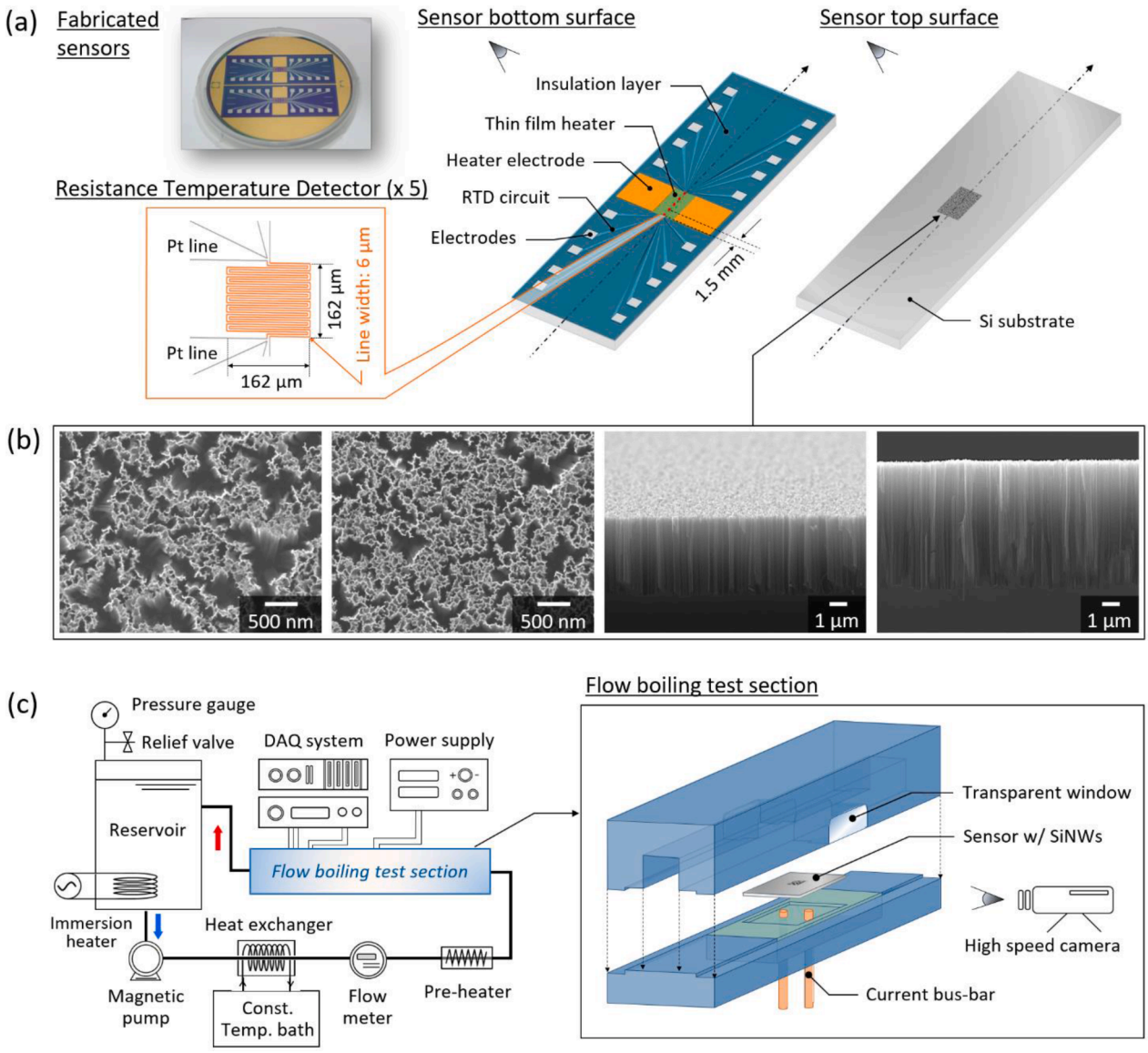

Fig. 2. Materials and experimental apparatus utilized in this study. (a) The sensor chip, equipped with local temperature measuring resistive temperature detectors (RTDs) with *in-situ* SiNWs, designed for characterizing flow boiling performance. (b) Vertically aligned monolithic SiNWs with an average height of 6.8 μm. (c) The experimental apparatus, including a test section where the sensor is installed, designed for the evaluation of flow boiling performance.

that could influence the heat transfer results. Our choice reflects common conditions in industrial applications, thus ensuring the relevance of our findings.

The flow boiling system operated as a closed loop, where the working fluid in the main reservoir was continuously stirred. The working fluid was stored in the main reservoir and mixed continuously by a stirrer. Dissolved gases in the working fluid were removed by a preceding degassing process for 2 h. The degassed convective flow was circulated by a magnetic pump (TXS5.3, Tuthill Co.) and an electric motor (LG-OTIS) to attain the controlled Reynolds number. The mass flow rate was monitored by a flowmeter (Ultramass MK II, Oval Co.). Data signals including local temperatures on a boiling surface, measured from the RTDs, were recorded using data acquisition systems (SCXI-1503, National Instruments and 34970A, Agilent Technologies) and a desktop computer. A high-speed camera (Speedsense M110, Dantec) was positioned horizontally at the height of the boiling surface to observe bubble behavior. Single bubble behavior was observed and recorded at a frame rate of 2000 Hz near the onset of nucleate boiling.

2.4. Liquid accessibility characterization

The surface tension of the liquid was manipulated by varying concentrations of a nonionic fluorosurfactant (FS-3100, DuPont). This surfactant, stable under acidic conditions and non-flammable, was used at concentrations ranging from 0 to 1000 ppm, reducing the liquid surface tension from 72 to 16 mN/m. The surfactant's critical micelle concentration (CMC) was identified as 100 ppm. A slight increase in dynamic viscosity by 5% was also noted. Contact angles (CAs) were measured using a contact angle measuring system (KSV CAM-200, KSV Ins.), with droplet images captured at a 2 ms frame interval. Measurements were conducted using 2.5 μL droplets of DI water and the surfactant solutions, with the process repeated five times to obtain the average CAs for each case. For hemi-wicking rate evaluation, SiNW-coated substrates were immersed in DI water and surfactant solutions of various concentrations. Hemi-wicking behavior was recorded using a high-speed camera (Speedsense M110, Dantec) with a pixel resolution of 25 pixels/mm and a time interval of 2000 fps. The wicking distance was determined through post-imaging processing and averaged from at least three samples with SiNW-forested surfaces.

2.5. Data reduction for local heat transfer evaluation

The applied heat flux was estimated by measuring the current and voltage drop through the ITO thin-film heater:

$$q'' = Q / A_{heater} = (V \cdot I - Q_{loss}) / A_{heater} \quad (2)$$

where q'', Q, A_{heater}, V, I, and Q_{loss} are the heat flux, applied power, heating area, voltage drop, current, and loss of the applied power, respectively. The heat loss was small because the Si substrate used for the sensor chip had a high thermal conductivity of 140 W/m·K and a thickness of only 500 μm. However, we evaluated the heat loss to improve the reliability of our experimental results. The loss of the applied power was evaluated by considering heat spreading through the silicon substrate. The conductive heat loss through a silicon substrate, which has relatively high thermal conductivity, is analyzed by three-dimensional numerical analyses under a steady state condition using a commercial CFD code (ANSYS Fluent 2020R2) to determine the uncertainty estimation of the applied heat flux [52,57]. The heat flux

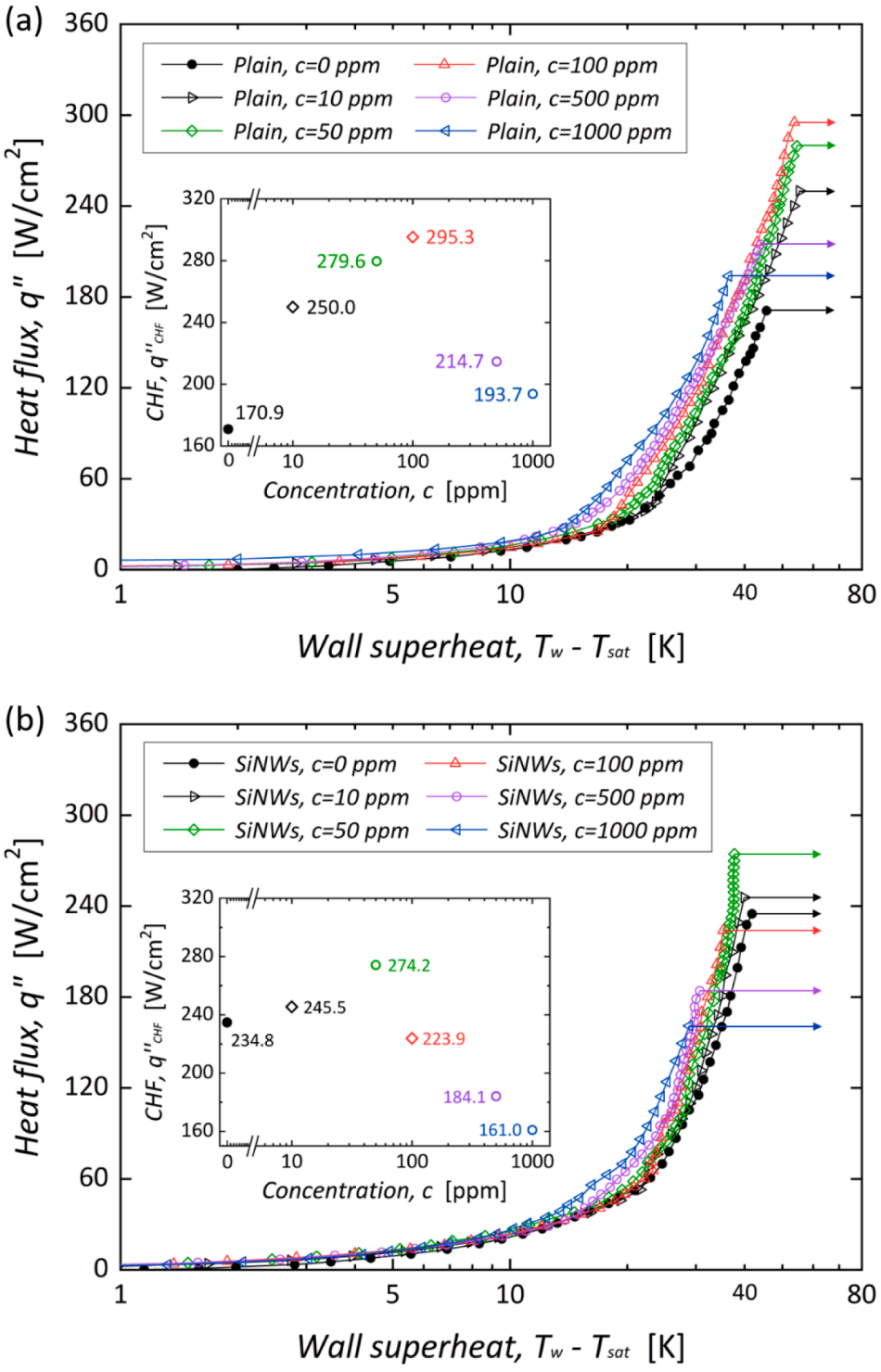

Fig. 3. Flow boiling curves for various surfactant concentrations *c*. (a) Boiling curves on a smooth surface and (b) on a roughened surface featuring 6.8 μm tall SiNWs. Arrows mark the corresponding CHF values, with inset graphs quantifying the CHF for each concentration.

deviation due to spreading is considered conductive heat loss, and the evaluated heat loss uncertainty is 3.43%.

The resistance of the RTDs fabricated on the thin-film heater changed according to the temperature. Thus, a resistance–temperature correlation was determined before the experiments for each RTD. According to the correlation function, the temperature from each RTD was evaluated, and the wall temperature at the boiling surface was evaluated by Fourier 1-D conduction across the substrate thickness:

$$T_w = T_{RTD} - (t_{Si} / k_{Si}) \cdot q'', \tag{3}$$

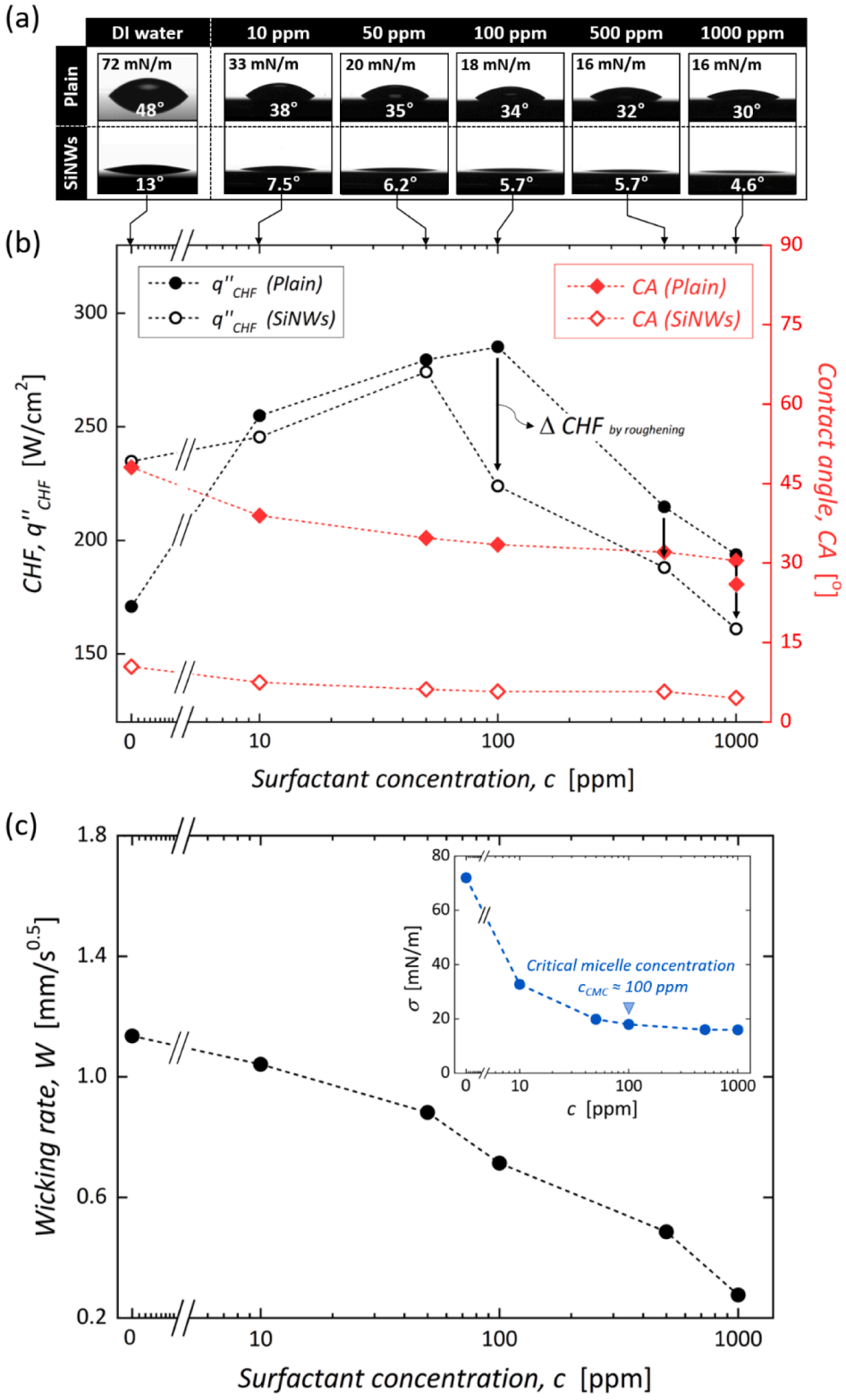

Fig. 4. (a) Apparent CAs on smooth and nanowire surfaces at various surfactant concentrations. (b) The distribution of CHF changes as surfactant concentration increases, weakening the wicking phenomenon. Solid and open symbols denote results from smooth and nanowire surfaces, respectively. (c) Wicking rate W plotted with surfactant concentration. The inset graph illustrates the surface tension alteration due to surfactant addition.

where, T_w, T_{RTD}, t_{Si}, and k_{Si} are the wall temperature on the boiling surface, the temperature from the RTD, the thickness of the Si substrate, and the thermal conductivity of the substrate, respectively [52]. In order to ensure comprehensive understanding and transparency, we have elaborated on the uncertainties encountered during the sensor fabrication process and data reduction in the Supporting Information (SI). This includes a detailed analysis of uncertainties associated with the dimensions handled during sensor processing, and the uncertainties of key heat transfer indices derived from data reduction.

3. Results and discussion

In this section, we discuss the results obtained from our experiments and their implications on the understanding of flow boiling heat transfer. We delve into the effects of surface roughening and hemi-wicking on CHF and bubble dynamics, highlighting their interplay and individual contributions. This section also explores the functionalized interface, the phenomenon of hemi-wicking caused by surface roughening, and its impact on anti-pinning of bubbles. These discussions provide insights into the mechanisms governing flow boiling on nanostructured surfaces, contributing to the advancement of thermal management technologies.

3.1. Classical viewpoint on roughening, static wetting, and surface tension upon boiling

Fig. 3 depicts characteristic boiling curves obtained during flow boiling from plain (smooth) and nano-inspired surfaces. The observed boiling characteristics are predominantly influenced by two factors: *surface roughness* and *liquid accessibility* [58]. Notably, compared to the boiling curves for smooth surfaces (Fig. 3a), the curves for the nano-inspired surfaces (Fig. 3b) are shifted to the left. This underscores the significant impact of nanoscale surface roughening on boiling [26,28]. Monolithic SiNWs, characterized by high aspect ratios, create a distinctively rough morphology with secondary microscale cavities. This unique structure effectively catalyzes ebullition within nucleate boiling regimes while concurrently reducing wall superheat [23,24,26,49]. Furthermore, we also manipulated the liquid accessibility by adding surfactants (FS-3100, DuPont). As the surfactant concentration increased, the boiling curves for both surfaces shifted leftward, indicating reduced wall superheats. This shift suggests that decreasing the liquid's surface tension, thereby replenishing the liquid, contributes to the reduction of superheat [59,60].

Enhanced liquid accessibility increases the CHF by facilitating the penetration of liquid into spaces between vapor bubbles, which prevents bubble coalescence and delays the onset of film boiling [61,62]. A reduction in surface tension imparts hydrophilic characteristics at interfaces, resulting in a decrease in apparent CA as described by Young's equation $\cos\theta=(\sigma_{SG}-\sigma_{SL})/\sigma$, where σ_{SG}, σ_{SL}, and σ represent the solid-gas, solid-liquid, and liquid-gas surface tension, respectively [38,63]. Fig. 4a illustrates that lowering surface tension enhances liquid accessibility with reduced static CA on both smooth and nano-inspired surfaces. At a surfactant concentration of 100 ppm on the smooth surface, the CA drops to 34° and further approaches 30° at 1000 ppm. Nano-inspired surfaces, inherently superhydrophilic, exhibit less sensitivity to changes in surfactant concentration, with CA altering from 13° without surfactants to 4.6° at 1000 ppm. This relative insensitivity to surfactant concentration is attributed to the lower CA induced by surface morphology, consistent with Wenzel's model [40,64].

The traditional perspective on boiling heat transfer posits that enhanced hydrophilic wetting leads to an increase in CHF. For instance, the assessment by Dhir and Liaw of the interfacial thermal boundary layer and sequential mass equilibrium in relation to CA supports the notion that CHF enhancement is proportional to increased hydrophilicity [65]. Consequently, as the concentration of surfactant increases, a stronger CHF is anticipated on smooth surfaces (Fig. 3a) compared to nano-inspired surfaces (Fig. 3b).

With a further increase in the surfactant concentration, the CHF does not exhibit a corresponding rise; instead, it shows a reduction for both smooth and nano-inspired surfaces, as illustrated in Fig. 4b. This decline in CHF is attributed to the increased dynamic viscosity of the liquid, a consequence of high surfactant concentrations [61,66]. When the surfactant concentration exceeds the critical micelle concentration (CMC), surfactant molecules start forming micelles, resulting in increased dynamic viscosity of the working fluid (see Figure S2b in SI) [67,68]. This increase in viscosity impedes liquid accessibility, clarifying why the maximum surfactant concentration does not align with the peak CHF for either surface. Importantly, in the vicinity of the boiling surface where evaporation is predominant, the local concentration of surfactants is likely to be much higher due to the water evaporation. This localized surge in surfactant concentration could intensify the dynamic viscosity near the boiling surface, potentially exacerbating the reduction in liquid accessibility and further decreasing the CHF, especially on nanostructured surfaces. The maximum CHFs are observed at 100 ppm for smooth surfaces and 50 ppm for nano-inspired surfaces, with the latter demonstrating enhanced CHF at lower surfactant concentrations due to its inherent hydrophilic characteristics. These findings are consistent with previous discussions: dissolved surfactants enhance liquid accessibility to the boiling surface, leading to lower CAs and delayed bubble coalescence [58,59,61,69,70], ultimately improving CHF. However, when surfactant concentrations surpass the CMC, the resultant increase in dynamic viscosity adversely affects CHF.

3.2. Functionalized interface: hemi-wicking caused by surface roughening

While both surface roughening and liquid accessibility are recognized as crucial determinants of boiling performance, the extent to which these factors independently or synergistically influence CHF is still ambiguous. The conventional approach inadequately addresses the contributions of roughness factor (r) or apparent CA (θ) in evaluating boiling performance. For instance, although a reduction in CA – achieved either through decreasing surface tension or introducing highly rough nanostructures – should theoretically result in an increased CHF, this explanation falls short of accounting for the substantial enhancement observed on both smooth and nano-inspired surfaces [26]. The traditional perspective does not establish a definitive correlation between apparent CA and CHF, suggesting a need for further investigation into whether the identified factors are truly independent or if any additional, unidentified influencing factors exist.

Nanostructures and combined nano/micro-hybrid structures at the solid-liquid interface markedly increase surface roughness, which expands the solid-liquid contact area and facilitates heat dissipation. As noted earlier, increased roughness augments hydrophilicity by decreasing the CA, as outlined by Wenzel's model [40]. A less appreciated factor is *hemi-wicking*, which refers to the capillary-driven spread of liquid across a roughened interface due to its morphology. The occurrence of hemi-wicking is governed by the substrate's inherent surface free energy and its roughness factor [71]. It manifests when the force balance at the liquid-solid interface equilibrium meets specific geometric prerequisites [38,71], represented by:

$$cos^{-1}(\theta_c) = cos^{-1}((1-\varphi)/(r-\varphi)) > \theta^*, \tag{3a}$$

where θ_c denotes the critical CA. Using Washburn's model [72,73], hemi-wicking can be quantified via the wicking rate, W:

$$W \propto \left(\frac{2H}{3\beta}\frac{\sigma}{\mu}\frac{\cos\theta^* - \cos\theta_c}{\cos\theta_c}\right)^{1/2}, \tag{4}$$

where H, β, and μ represent the height of the interfacial structures, shape factor, and fluid dynamic viscosity, respectively. Herein, the shape factor β is defined as a parameter reflecting the dimensions and shape of capillary-inducing structures, aligning with the definitions provided in

previous studies [10,42,46,73]. The wicking rate is determined by both the fluid's properties and the surface energy balance, as well as geometric parameters associated with shape factors and dimensions.

It is crucial to note that "surface roughness" should not be viewed as a standalone parameter when assessing boiling performance. Rather, it serves as an indicator of hemi-wicking, which is intrinsically tied to the spread of liquid and roughness itself. To discern the sole impact of roughness, one approach is to reduce the liquid's surface tension on a wicking surface, thereby eliminating the wicking effect. The formation of micelles resulting from increased viscosity further inhibits hemi-wicking since viscosity and wicking rate are inversely related. This increased viscosity disrupts liquid propagation among nanostructures, thereby attenuating hemi-wicking. As suggested by Eq. (3), by lowering the surface tension of DI water, it is possible to reduce hemi-wicking while preserving the roughness (as shown in Fig. 4c). Notably, a 77% decline in the wicking rate was observed when the surfactant concentration increased from zero to 1000 ppm. This method allows us to pinpoint the exclusive effect of surface roughness by decoupling it from

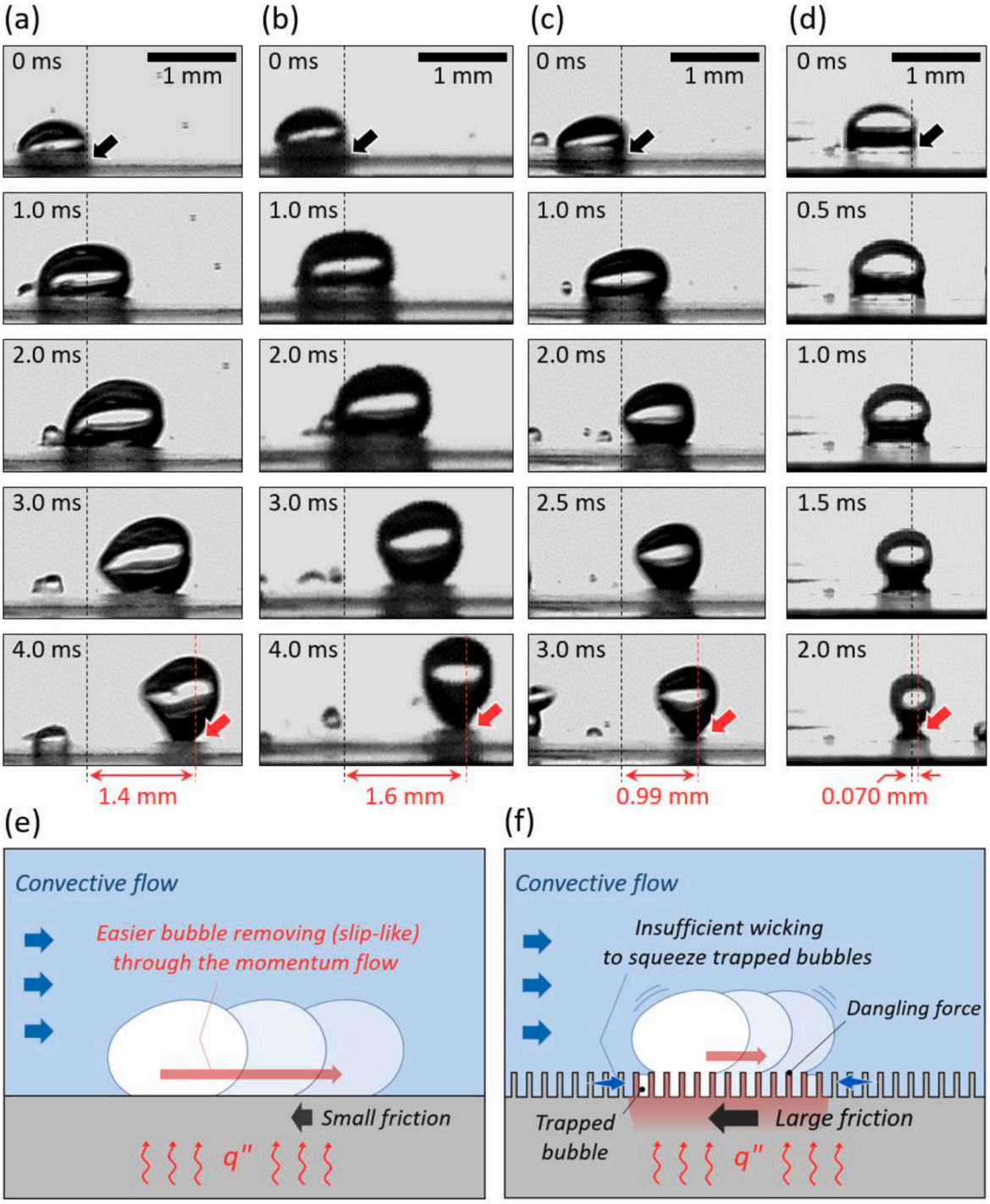

Fig. 5. Visualization of bubble pinning (at 0 ms) post-growth and subsequent departure from smooth surfaces at surfactant concentrations of (a) 0 ppm and (b) 100 ppm, and roughened surfaces at surfactant concentrations of (c) 0 ppm and (d) 100 ppm. Black dashed lines and arrows mark the initial pinning position at the rear of forming bubbles, while red arrows indicate the final departure position. Schematic diagrams in (e) and (f) illustrate flow resistance variations depending on interface conditions on smooth and roughened surfaces, respectively.

hemi-wicking, unlike previous studies that inherently linked roughness effects with wicking [4,10,13,16,22,24,74].

3.3. Hemi-wicking for anti-pinning of bubbles

By decoupling/diminishing the hemi-wicking effect, the morphological influence of SiNWs can be reinterpreted as a unilateral roughness effect along the *x*-axis of Figs. 4b and 4c. For instance, in the absence of surfactants (at 0 ppm), the nano-inspired surface exhibits a CHF 37% higher than a smooth surface due to hemi-wicking and is consistent with previous studies [36,75]. However, this same nano-inspired surface shows an 11.3% decrease in CHF compared to the smooth surface at surfactant concentrations ranging from 10 to 1000 ppm. While nanowires are generally believed to enhance CHF by reducing the CA [14], our findings indicated a significant reduction in CHF when the roughness effect of nanowires is considered separately, without the influence of wicking. This reduction might be more pronounced due to a localized increase in surfactant concentration, leading to increased viscosity at the boiling surface. In a

During forced convection in flow boiling, we observed that surface roughening impeded bubble detachment as a plausible reason for the CHF reduction on the roughened surfaces. Bubbles on various surfaces exhibited distinct slip distances under lateral forced convection, as illustrated in Fig. 5. On smooth surfaces, bubbles slid far downstream (1.4–1.6 mm, Figs. 5a and 5b) regardless of surfactant concentration. In contrast, on roughened surfaces, bubbles had shorter slip distances (Figs. 5c and 5d), which further decreased as surfactant concentration increased, reducing secondary hemi-wicking. The observed differences in bubble behavior are not solely due to the presence of surfactant. When surfactants adhere to silicon in water, they form a bilayer on the silicon surface, exposing their hydrophilic head to the water [76]. This promotes water movement around the silicon and aids in liquid supply between nanowires without reducing slip distance on nanostructure surfaces.

The primary factor driving bubble detachment from boiling surfaces is forced flow. As bubbles move, their behavior is influenced by surface morphology. Bubbles nucleated on nano-inspired surfaces are typically smaller and tend to merge as boiling intensifies [24,77]. When hemi-wicking is active, the continuous influx of liquid pushes the vapor beneath the bubble, enabling easier bubble movement, even on the roughened surfaces. In the absence of hemi-wicking, vapor can be trapped within the roughened interface, leading to larger bubbles that cling to the surface [78]. Interestingly, roughened surfaces extend the contact lines, creating a force that keeps bubbles anchored. This increased adhesion, a consequence of the rougher morphology (Fig. 5f), impedes bubble detachment, a behavior contrasting with that seen on smooth surfaces (Fig. 5e) which facilitates easier bubble release. This is reminiscent of the pinning effect seen with droplets on textured surfaces [79,80]. Such roughened surfaces interfere with the movement of the three-phase contact line, thus making bubble removal more challenging. This effect delays the supply of fresh liquid to initial nucleation sites until the bubble detaches, particularly when hemi-wicking is lacking (Fig. 5d).

On smooth surfaces, bubble dynamics are mainly driven by convective flow, which cools the initial nucleation site as the bubble moves (Fig. 5b). The adherence of bubbles to roughened surfaces highlights the negative impact of separating roughening and hemi-wicking (Figs. 5c and 5d). This adherence, as presented by the shortened slip distance from Figs. 5c to 5d, thickens the vapor layer before film boiling starts, raising thermal resistance and hindering heat dissipation. This phenomenon explains the lower CHF observed on nano-inspired surfaces and the progressive decrease in CHF despite reduced surface tension. Therefore, it is essential to recognize the *reversal* effect tied to surface roughening. Employing hemi-wicking to minimize bubbles trapped within roughened surfaces emerges as a viable solution in boiling applications.

In addition to our observations on hemi-wicking and bubble pinning, it is pertinent to consider the implications for flow boiling instabilities. While our study did not directly focus on flow instabilities, the interplay between nanoscale surface structures, hemi-wicking, and bubble dynamics could provide valuable insights into this phenomenon [81–83]. For instance, the controlled hemi-wicking on nanostructured surfaces might contribute to stabilizing the flow by moderating bubble coalescence and movement, potentially mitigating flow boiling instabilities [82–86]. This aspect warrants further investigation, particularly considering the prevalence of such instabilities in microchannel configurations and their impact on thermal performance. Therefore, our findings on surface modifications and hemi-wicking could provide a foundation for future studies aimed at comprehensively understanding and managing convective flow boiling instabilities in various cooling systems [87,88].

4. Conclusions

This study significantly advanced our understanding of flow boiling by exploring the synergistic effects of morphological roughening and hemi-wicking through SiNWs on CHF. We successfully differentiated the roles of surface roughening and hemi-wicking by manipulating liquid surface tension with surfactants. Our experimental findings revealed a notable 37% increase in CHF on nano-inspired surfaces compared to their smooth counterparts, demonstrating the benefits of enhanced liquid accessibility, dynamic hemi-wicking, and decreased static contact angle.

Conversely, the suppression of hemi-wicking resulted in an 11.3% decrease in CHF, even on nanowire-inspired surfaces. This observation emphasizes the crucial role of hemi-wicking in facilitating bubble removal and its positive impact on CHF enhancement. In the absence of hemi-wicking, surface roughening can impede bubble detachment in forced convection, highlighting the previously overlooked significance of hemi-wicking.

The insights gained from this study suggest that future boiling studies should design surface morphologies that optimize bubble detachment while considering the potential adverse effects of surface roughening. The role of hemi-wicking in managing bubbles on rough surfaces is pivotal for boiling applications. This study not only advances our understanding of nanostructuring for thermal management but also sets the stage for future research focused on optimizing bubble detachment and heat dissipation in high-efficiency cooling technologies, laying a robust groundwork for subsequent studies on heat transfer and boiling mechanisms.

CRediT authorship contribution statement

Geehong Choi: Writing – review & editing, Writing – original draft, Visualization, Investigation, Formal analysis, Data curation, Conceptualization. **Beom Seok Kim:** Writing – review & editing, Writing – original draft, Visualization, Validation, Investigation, Funding acquisition, Formal analysis, Data curation, Conceptualization. **Maroosol Yun:** Validation, Methodology, Formal analysis, Data curation. **Namkyu Lee:** Methodology, Investigation, Formal analysis, Data curation. **Sangwoo Shin:** Writing – review & editing, Writing – original draft, Formal analysis, Data curation, Conceptualization. **Hyung Hee Cho:** Writing – review & editing, Writing – original draft, Supervision, Resources, Project administration, Formal analysis, Conceptualization.

Declaration of competing interest

All the authors, G. Choi, B. S. Kim, M. Yun, N. Lee, S. Shin, and H. H. Cho, declare that there are no competing interests.

Data availability

Data will be made available on request.

Acknowledgments

This work was supported by the Human Resources Development program (No.20204030200110) through a Korea Institute of Energy Technology Evaluation and Planning (KETEP) grant funded by the Ministry of Trade, Industry, and Energy of the Korean Government. This work was supported by a grant from the National Research Foundation of Korea (NRF) funded by the Ministry of Science and Information and Communications (MSIT) of the Korean Government (No. 2021R1F1A1062420). This study was financially supported by Seoul National University of Science and Technology.

Supplementary materials

Supplementary material associated with this article can be found, in the online version, at doi:10.1016/j.ijmecsci.2024.109021.

References

[1] Luo J, Wu S-Y, Xiao L, Zhou S-Y, Chen Z-L. Transient boiling heat transfer mechanism of droplet impacting heated cylinder. Int J Mech Sci 2022;233:107675.
[2] Liang G, Mudawar I. Review of nanoscale boiling enhancement techniques and proposed systematic testing strategy to ensure cooling reliability and repeatability. Appl Therm Eng 2021;184:115982.
[3] Moghadasi H, Saffari H. Experimental study of nucleate pool boiling heat transfer improvement utilizing micro/nanoparticles porous coating on copper surfaces. Int J Mech Sci 2021;196:106270.
[4] Li J, Zhao Y, Ma J, Fu W, Yan X, Rabbi KF, Miljkovic N. Superior Antidegeneration Hierarchical Nanoengineered Wicking Surfaces for Boiling Enhancement. Adv Funct Mater 2021;31:2108836.
[5] Hsu W-T, Lee D, Lee N, Yun M, Cho HH. Enhancement of flow boiling heat transfer using heterogeneous wettability patterned surfaces with varying inter-spacing. Int J Heat Mass Transfer 2021;164:120596.
[6] Moon JH, Fadda D, Shin DH, Kim JS, Lee J, You SM. Boiling-driven, wickless, and orientation-independent thermal ground plane. Int J Heat Mass Transfer 2021;167:120817.
[7] Shin S, Choi G, Rallabandi B, Lee D, Shim DI, Kim BS, Kim KM, Cho HH. Enhanced boiling heat transfer using self-actuated nanobimorphs. Nano Lett 2018;18:6392–6.
[8] Dhillon NS, Buongiorno J, Varanasi KK. Critical heat flux maxima during boiling crisis on textured surfaces. Nat Commun 2015;6:8247.
[9] Liang G, Mudawar I. Pool boiling critical heat flux (CHF) – Part 1: review of mechanisms, models, and correlations. Int J Heat Mass Transfer 2018;117:1352–67.
[10] Kim BS, Lee H, Shin S, Choi G, Cho HH. Interfacial wicking dynamics and its impact on critical heat flux of boiling heat transfer. Appl Phys Lett 2014;105:191601.
[11] Chu K-H, Joung YS, Enright R, Buie CR, Wang EN. Hierarchically structured surfaces for boiling critical heat flux enhancement. Appl Phys Lett 2013;102:151602.
[12] Li J, Zhu G, Kang D, Fu W, Zhao Y, Miljkovic N. Endoscopic visualization of contact line dynamics during pool boiling on capillary-activated copper microchannels. Adv Funct Mater 2021;31:2006249.
[13] Cho HJ, Preston DJ, Zhu Y, Wang EN. Nanoengineered materials for liquid–vapour phase-change heat transfer. Nat Rev Mater 2016;2:16092.
[14] Kandlikar SG. A theoretical model to predict pool boiling CHF incorporating effects of contact angle and orientation. J Heat Transfer 2001;123:1071–9.
[15] Zuber N.Y. Hydrodynamic aspects of boiling heat transfer. AEC Report AECU-4439 1959.
[16] Shim DI, Hsu W-T, Yun M, Lee D, Kim BS, Cho HH. Superbiphilic patterned nanowires with wicking for enhanced pool boiling heat transfer. Int J Mech Sci 2023;249:108280.
[17] Choi G, Yun M, Hsu W-T, Shim DI, Lee D, Kim BS, Cho HH. Enhanced boiling heat transfer by nucleation patterning with self-assembly of reduced graphene oxide coating. Int J Heat Mass Transfer 2022;197:123329.
[18] Heidary A, Moghadasi H, Saffari H. Impact of dimensional characteristics of low-conductive channels on the enhancement of pool boiling: an experimental analysis. Int J Mech Sci 2021;209:106710.
[19] Mehdikhani A, Moghadasi H, Saffari H. An experimental investigation of pool boiling augmentation using four-step electrodeposited micro/nanostructured porous surface in distilled water. Int J Mech Sci 2020;187:105924.
[20] Li J, Fu W, Zhang B, Zhu G, Miljkovic N. Ultrascalable Three-Tier Hierarchical Nanoengineered Surfaces for Optimized Boiling. ACS Nano 2019;13:14080–93.
[21] Choi G, Shim DI, Lee D, Kim BS, Cho HH. Enhanced nucleate boiling using a reduced graphene oxide-coated micropillar. Int Commun Heat Mass Transfer 2019;109:104331.
[22] Zhang C, Palko JW, Barako MT, Asheghi M, Santiago JG, Goodson KE. Enhanced capillary-fed boiling in copper inverse opals via template sintering. Adv Funct Mater 2018;28:1803689.
[23] Shin S, Choi G, Kim BS, Cho HH. Flow boiling heat transfer on nanowire-coated surfaces with highly wetting liquid. Energy 2014;76:428–35.
[24] Kim BS, Shin S, Lee D, Choi G, Lee H, Kim KM, Cho HH. Stable and uniform heat dissipation by nucleate-catalytic nanowires for boiling heat transfer. Int J Heat Mass Transfer 2014;70:23–32.
[25] Ahn HS, Jang J-W, Seol M, Kim JM, Yun D-J, Park C, Kim H, Youn DH, Kim JY, Park G, Park SC, Kim JM, Yu DI, Yong K, Kim MH, Lee JS. Self-assembled foam-like graphene networks formed through nucleate boiling. Sci Rep 2013;3:1396.
[26] Chen R, Lu MC, Srinivasan V, Wang Z, Cho HH, Majumdar A. Nanowires for enhanced boiling heat transfer. Nano Lett 2009;9:548–53.
[27] Song J, Cheng W, Nie M, He X, Nam W, Cheng J, Zhou W. Partial Leidenfrost evaporation-assisted ultrasensitive surface-enhanced Raman spectroscopy in a Janus water droplet on hierarchical plasmonic micro-/nanostructures. ACS Nano 2020;14:9521–31.
[28] Li C, Wang Z, Wang PI, Peles Y, Koratkar N, Peterson GP. Nanostructured copper interfaces for enhanced boiling. Small 2008;4:1084–8.
[29] Lu MC, Chen RK, Srinivasn V, Carey V, Majumdar A. Critical heat flux of pool boiling on Si nanowire array-coated surfaces. Int J Heat Mass Transfer 2011;54:5359–67.
[30] Bourdon B, Rioboo R, Marengo M, Gosselin E, De Coninck J. Influence of the wettability on the boiling onset. Langmuir 2012;28:1618–24.
[31] Liu TY, Li PL, Liu CW, Gau C. Boiling flow characteristics in microchannels with very hydrophobic surface to super-hydrophilic surface. Int J Heat Mass Transfer 2011;54:126–34.
[32] Takata Y, Hidaka S, Cao JM, Nakamura T, Yamamoto H, Masuda M, Ito T. Effect of surface wettability on boiling and evaporation. Energy 2005;30:209–20.
[33] Wen DS, Wang BX. Effects of surface wettability on nucleate pool boiling heat transfer for surfactant solutions. Int J Heat Mass Transfer 2002;45:1739–47.
[34] Hanley H, Coyle C, Buongiorno J, McKrell T, Hu L-W, Rubner M, Cohen R. Separate effects of surface roughness, wettability, and porosity on the boiling critical heat flux. Appl Phys Lett 2013;103:024102.
[35] Betz AR, Jenkins J, Kim C-J, Attinger D. Boiling heat transfer on superhydrophilic, superhydrophobic, and superbiphilic surfaces. Int J Heat Mass Transfer 2013;57:733–41.
[36] Hsu C-C, Chen P-H. Surface wettability effects on critical heat flux of boiling heat transfer using nanoparticle coatings. Int J Heat Mass Transfer 2012;55:3713–9.
[37] Rosario R, Gust D, Garcia AA, Hayes M, Taraci JL, Clement T, Dailey JW, Picraux ST. Lotus effect amplifies light-induced contact angle switching. J Phys Chem B 2004;108:12640–2.
[38] Kim BS, Shin S, Shin SJ, Kim KM, Cho HH. Control of superhydrophilicity/superhydrophobicity using silicon nanowires via electroless etching method and fluorine carbon coatings. Langmuir 2011;27:10148–56.
[39] Cheng H-C, Chang T-L, Chen P-H. Experimental investigation of inner bubble dynamics during water droplet evaporation from heated surfaces with different roughness and wettability levels. Int J Heat Mass Transfer 2020;157:119980.
[40] Wenzel RN. Resistance of solid surfaces to wetting by water. Ind Eng Chem 1936;28:988–94.
[41] Chu K-H, Enright R, Wang EN. Structured surfaces for enhanced pool boiling heat transfer. Appl Phys Lett 2012;100:241603.
[42] Mai TT, Lai CQ, Zheng H, Balasubramanian K, Leong KC, Lee PS, Lee C, Choi WK. Dynamics of wicking in silicon nanopillars fabricated with interference lithography and metal-assisted chemical etching. Langmuir 2012;28:11465–71.
[43] Wang Z, Zhao J, Bagal A, Dandley EC, Oldham CJ, Fang T, Parsons GN, Chang C-H. Wicking enhancement in three-dimensional hierarchical nanostructures. Langmuir 2016;32:8029–33.
[44] Ahn HS, Park G, Kim J, Kim MH. Wicking and spreading of water droplets on nanotubes. Langmuir 2012;28:2614–9.
[45] Quéré D. Wetting and roughness. Annu Rev Mater Res 2008;38:71–99.
[46] Ishino C, Reyssat M, Reyssat E, Okumura K, Quéré D. Wicking within forests of micropillars. Europhys Lett 2007;79:56005.
[47] Extrand CW, Moon SI, Hall P, Schmidt D. Superwetting of structured surfaces. Langmuir 2007;23:8882–90.
[48] Agapov RL, Boreyko JB, Briggs DP, Srijanto BR, Retterer ST, Collier CP, Lavrik NV. Asymmetric wettability of nanostructures directs Leidenfrost droplets. ACS Nano 2014;8:860–7.
[49] Li D, Wu GS, Wang W, Wang YD, Liu D, Zhang DC, Chen YF, Peterson GP, Yang R. Enhancing flow boiling heat transfer in microchannels for thermal management with monolithically-integrated silicon nanowires. Nano Lett 2012;12:3385–90.
[50] Hsu W-T, Lee N, Yun M, Lee D, Cho HH. Unidirectional wicking-driven flow boiling on tilted pillar structures for high-power applications. Int J Heat Mass Transfer 2022;189:122673.
[51] Lee D, Lee N, Shim DI, Kim BS, Cho HH. Enhancing thermal stability and uniformity in boiling heat transfer using micro-nano hybrid surfaces (MNHS). Appl Therm Eng 2018;130:710–21.
[52] Choi G, Kim BS, Lee H, Shin S, Cho HH. Jet impingement in a crossflow configuration: convective boiling and local heat transfer characteristics. Int J Heat Fluid Flow 2014;50:378–85.
[53] Huang Z, Geyer N, Werner P, de Boor J, Gösele U. Metal-assisted chemical etching of silicon: a review. Adv Mater 2011;23:285–308.
[54] Kim S-M, Khang D-Y. Bulk micromachining of Si by metal-assisted chemical etching. Small 2014;10:3761–6.

[55] Kim BS, Shin S, Shin SJ, Kim KM, Cho HH. Micro-nano hybrid structures with manipulated wettability using a two-step silicon etching on a large area. Nanoscale Res Lett 2011;6:333.
[56] Kim BS, Choi G, Shin S, Gemming T, Cho HH. Nano-inspired fluidic interactivity for boiling heat transfer: impact and criteria. Sci Rep 2016;6:34348.
[57] Kim BS, Choi G, Shim DI, Kim KM, Cho HH. Surface roughening for hemi-wicking and its impact on convective boiling heat transfer. Int J Heat Mass Transfer 2016;102:1100–7.
[58] Raza MQ, Kumar N, Raj R. Surfactants for bubble removal against buoyancy. Sci Rep 2016;6:19113.
[59] Cho HJ, Mizerak JP, Wang EN. Turning bubbles on and off during boiling using charged surfactants. Nat Commun 2015;6:8599.
[60] Shoghl SN, Bahrami M. Experimental investigation on pool boiling heat transfer of ZnO, and CuO water-based nanofluids and effect of surfactant on heat transfer coefficient. Int Commun Heat Mass Transfer 2013;45:122–9.
[61] Jeong YH, Sarwar MS, Chang SH. Flow boiling CHF enhancement with surfactant solutions under atmospheric pressure. Int J Heat Mass Transfer 2008;51:1913–9.
[62] Shin S, Kim BS, Choi G, Lee H, Cho HH. Double-templated electrodeposition: simple fabrication of micro-nano hybrid structure by electrodeposition for efficient boiling heat transfer. Appl Phys Lett 2012;101:251909.
[63] Boreyko JB, Baker CH, Poley CR, Chen C-H. Wetting and dewetting transitions on hierarchical superhydrophobic surfaces. Langmuir 2011;27:7502–9.
[64] Martines E, Seunarine K, Morgan H, Gadegaard N, Wilkinson CDW, Riehle MO. Superhydrophobicity and superhydrophilicity of regular nanopatterns. Nano Lett 2005;5:2097–103.
[65] Dhir VK, Liaw SP. Framework for a unified model for nucleate and transition pool boiling. J Heat Transfer 1989;111:739–46.
[66] Wu W-T, Yang Y-M, Maa J-R. Nucleate pool boiling enhancement by means of surfactant additives. Exp Therm Fluid Sci 1998;18:195–209.
[67] Tyuzyo K. On the relation between viscosity and critical micelle concentration of detergent solutions. Kolloid-Zeitschrift 1961;175:40–50.
[68] Wang S-C, Wei T-C, Chen W-B, Tsao H-K. Effects of surfactant micelles on viscosity and conductivity of poly(ethylene glycol) solutions. J Chem Phys 2004;120:4980–8.
[69] Jia H, Xu L, Xiao X, Zhong K. Study on boiling heat transfer of surfactant solution on grooved surface. Int J Heat Mass Transfer 2021;181:121876.
[70] Wang J, Li F-C, Li X-B. On the mechanism of boiling heat transfer enhancement by surfactant addition. Int J Heat Mass Transfer 2016;101:800–6.
[71] Lai CQ, Thompson CV, Choi WK. Uni-, bi-, and tri-directional wetting caused by nanostructures with anisotropic surface energies. Langmuir 2012;28:11048–55.
[72] Washburn EW. The dynamics of capillary flow. Phys Rev 1921;17:273–83.
[73] Lai CQ, Mai TT, Zheng H, Lee PS, Leong KC, Lee C, Choi WK. Influence of nanoscale geometry on the dynamics of wicking into a rough surface. Appl Phys Lett 2013;102:053104.
[74] Shim DI, Choi G, Lee N, Kim T, Kim BS, Cho HH. Enhancement of pool boiling heat transfer using aligned silicon nanowire arrays. ACS Appl Mater Interfaces 2017;9:17595–602.
[75] Morshed AKMM, Yang F, Yakut Ali M, Khan JA, Li C. Enhanced flow boiling in a microchannel with integration of nanowires. Appl Therm Eng 2012;32:68–75.
[76] Sharma KP, Aswal VK, Kumaraswamy G. Adsorption of nonionic surfactant on silica nanoparticles: structure and resultant interparticle interactions. J Phys Chem B 2010;114:10986–94.
[77] Lee D, Kim BS, Moon H, Lee N, Shin S, Cho HH. Enhanced boiling heat transfer on nanowire-forested surfaces under subcooling conditions. Int J Heat Mass Transfer 2018;120:1020–30.
[78] Khanikar V, Mudawar I, Fisher T. Effects of carbon nanotube coating on flow boiling in a micro-channel. Int J Heat Mass Transfer 2009;52:3805–17.
[79] Paxson AT, Varanasi KK. Self-similarity of contact line depinning from textured surfaces. Nat Commun 2013;4:1492.
[80] Bird JC, Dhiman R, Kwon H-M, Varanasi KK. Reducing the contact time of a bouncing drop. Nature 2013;503:385–8.
[81] Qu WL, Mudawar I. Flow boiling heat transfer in two-phase micro-channel heat sinks – I. Experimental investigation and assessment of correlation methods. Int J Heat Mass Transfer 2003;46:2755–71.
[82] Hedau G, Dey P, Raj R, Saha SK. Combined effect of inlet restrictor and nanostructure on two-phase flow performance of parallel microchannel heat sinks. Int J Therm Sci 2020;153:106339.
[83] Prajapati YK, Bhandari P. Flow boiling instabilities in microchannels and their promising solutions – a review. Exp Therm Fluid Sci 2017;88:576–93.
[84] Ferreira J, Kaviany M. Geometric-confinement suppression of flow-boiling instability using perforated wick: part I CHF and conductance enhancement. Int J Heat Mass Transfer 2020;159:120080.
[85] Liang G, Mudawar I. Review of channel flow boiling enhancement by surface modification, and instability suppression schemes. Int J Heat Mass Transfer 2020;146:118864.
[86] Kandlikar SG. Nucleation characteristics and instability considerations during flow boiling in microchannels. Exp Therm Fluid Sci 2006;30:441–7.
[87] Song J-Y, Senguttuvan S, Choi WW, Kim S-M. Effects of manifold design parameters on flow uniformity in parallel mini-channels. Int J Mech Sci 2022;234:107694.
[88] Zeng L, Deng D, Zhong N, Zheng G. Thermal and flow performance in microchannel heat sink with open-ring pin fins. Int J Mech Sci 2021;200:106445.